

First Search for Heavy Neutral Leptons with IceCube DeepCore

Dissertation

zur Erlangung des akademischen Grades
doctor rerum naturalium
(Dr. rer. nat.)

im Fach: Physik
Spezialisierung: Experimentalphysik

eingereicht an der
Mathematisch-Naturwissenschaftlichen Fakultät
der Humboldt-Universität zu Berlin

von

Leander Fischer M. Sc.
geboren am 24. Oktober 1992
in Heidelberg

Präsidentin der Humboldt-Universität zu Berlin
Prof. Dr. Julia von Blumenthal

Dekanin der Mathematisch-Naturwissenschaftlichen Fakultät
Prof. Dr. Caren Tischendorf

Copyright Notice

This book is released into the public domain using the CC-BY-4.0 code.

To view a copy of the CC-BY-4.0 code, visit:

<https://creativecommons.org/licenses/by/4.0/>

Colophon

This document was typeset with the help of KOMA-Script and L^AT_EX using the open-source kaobook template class.

The source code of this thesis is available at:

https://github.com/LeanderFischer/phd_thesis

Foreword

Before diving into the scientific content of my work, I would like to give some editorial remarks to smoothen the reading experience. Throughout the thesis, acronyms and experiment names are introduced in *italic font*, the first time they are mentioned, but are used in normal font from then on. The same goes for software packages, which are initially mentioned in SMALL CAPS FONT. One of the key features of the kaobok template - the big margin - is put to good use to house tables, figures, and additional notes, but also to highlight selected references. Of course, all references are listed in their full extent in the bibliography at the end, but additionally, some (but not necessarily all) of them will be highlighted in the margin next to where they appear to allow for an uninterrupted flow of reading.

Abstract

The observation of neutrino oscillations has established that neutrinos have non-zero masses. This phenomenon is not explained by the *standard model (SM)* of particle physics, but one viable explanation to this dilemma is the existence of *heavy neutral leptons (HNLs)* in the form of right-handed neutrinos. Depending on their mass and coupling to SM neutrinos, these particles could also play an important role in solving additional unexplained observations such as *dark matter (DM)* and the *baryon asymmetry of the universe (BAU)*. This work presents the first search for HNLs with the IceCube Neutrino Observatory. The standard three flavor neutrino model is extended by adding a fourth GeV-scale mass state and allowing mixing with the tau neutrino through the mixing parameter $|U_{\tau 4}|^2$. Three HNL mass values, m_4 , of 0.3 GeV, 0.6 GeV, and 1.0 GeV are tested using ten years of data, collected between 2011 and 2021, resulting in constraints for the mixing parameter of $|U_{\tau 4}|^2 < 0.19$ ($m_4 = 0.3$ GeV), $|U_{\tau 4}|^2 < 0.36$ ($m_4 = 0.6$ GeV), and $|U_{\tau 4}|^2 < 0.40$ ($m_4 = 1.0$ GeV) at 90 % confidence level. No significant signal of HNLs is observed for any of the tested masses. This first analysis lays the fundamental groundwork for future searches for HNLs in IceCube.

Zusammenfassung

The observation of neutrino oscillations has established that neutrinos have non-zero masses. This phenomenon is not explained by the *standard model (SM)* of particle physics, but one viable explanation to this dilemma is the existence of *heavy neutral leptons (HNLs)* in the form of right-handed neutrinos. Depending on their mass and coupling to SM neutrinos, these particles could also play an important role in solving additional unexplained observations such as *dark matter (DM)* and the *baryon asymmetry of the universe (BAU)*. This work presents the first search for HNLs with the IceCube Neutrino Observatory. The standard three flavor neutrino model is extended by adding a fourth GeV-scale mass state and allowing mixing with the tau neutrino through the mixing parameter $|U_{\tau 4}|^2$. Three HNL mass values, m_4 , of 0.3 GeV, 0.6 GeV, and 1.0 GeV are tested using ten years of data, collected between 2011 and 2021, resulting in constraints for the mixing parameter of $|U_{\tau 4}|^2 < 0.19$ ($m_4 = 0.3$ GeV), $|U_{\tau 4}|^2 < 0.36$ ($m_4 = 0.6$ GeV), and $|U_{\tau 4}|^2 < 0.40$ ($m_4 = 1.0$ GeV) at 90 % confidence level. No significant signal of HNLs is observed for any of the tested masses. This first analysis lays the fundamental groundwork for future searches for HNLs in IceCube.

Todo list

SB: there are more properties than just these. Somehow need a half sentence that explains why these are particularly important to single out (see ice papers for inspiration) (ORANGE)	2
CL: maybe define that absorption and scattering lengths are? they are defined differently so this invites a comparison that is not so obvious (ORANGE)	2
Add reference for the dust layer! Maybe also from the ice paper? mention/cite dust logger paper/procedure? (ORANGE)	2
exchange for figure with scattering (check abs/sca is correct) (ORANGE)	2
Add accuracy of the efficiency calibration here. (ORANGE)	3
Add angular profile plot (Summer agrees!) (create one based on Leif Radel as Alex did) (RED)	6
Add fractions of the different particle types in the bins for benchmark mass/mixing (another table?) (ORANGE)	10
fix caption (add description of what specific set number means (RED))	14
Need cite here! (RED)	15
I could add some final level effects of some systematics on the 3D binning and maybe discuss how they are different from the signal shape, or so? (ORANGE)	15
Find first occurrence of "Asimov" and add reference and explain it there (RED)	16
add 1-d data/mc agreement for example mass sample (0.6?) and all 3 analysis variables (RED)	18
add table with reduced chi2 for all 1-d distributions (RED)	18
fix caption and describe plot in text (RED)	18
Cite (again)! (RED)	18
Show best fit hole ice angular acceptance compared to nominal and flasher/in-situ fits, maybe? (YELLOW)	18
make summary plot (masses and mixing limits on one) and then discuss wrt to other experiments? (RED)	20

Contents

Foreword	iii
Abstract	v
Contents	ix
1 The IceCube Neutrino Observatory	1
1.1 Detector Components	1
1.1.1 Digital Optical Modules and the Antarctic Ice	2
1.1.2 IceCube Main-Array	3
1.1.3 DeepCore Sub-Array	4
1.2 Particle Propagation in Ice	4
1.2.1 Cherenkov Effect	4
1.2.2 Energy Losses	5
1.3 Event Morphologies	7
2 Search for Tau Neutrino Induced Heavy Neutral Lepton Events	9
2.1 Final Level Sample	9
2.1.1 Expected Rates/Events	9
2.1.2 Analysis Binning	10
2.2 Statistical Analysis	12
2.2.1 Test Statistic	12
2.2.2 Physics Parameters	13
2.2.3 Nuisance Parameters	13
2.2.4 Low Energy Analysis Framework	15
2.3 Analysis Checks	16
2.3.1 Minimization Robustness	16
2.3.2 Goodness of Fit	17
2.3.3 Data/MC Agreement	17
2.4 Results	18
2.4.1 Best Fit Nuisance Parameters	18
2.4.2 Agreement with Standard Model Three-Flavor Oscillation Measurement	18
2.4.3 Best Fit Parameters and Limits	19
2.4.4 Comparison to Other Experiments	20
2.5 Outlook	21
2.5.1 Shape Analysis Improvements	21
2.5.2 Test Coupling to Electron/Muon Flavor	21
2.5.3 Test Additional Coupling Processes	21
2.5.4 IceCube Upgrade	21
Figures	23
Tables	25
Bibliography	27

The IceCube Neutrino Observatory

1

The IceCube Neutrino Observatory [1] is a cubic-kilometer, ice-Cherenkov detector located at the geographic South Pole. IceCube utilizes the Antarctic glacial ice as detector medium to observe neutrinos by measuring the Cherenkov light produced from secondary charged particles. It was deployed between 2006 and 2011 and has been taking data since the installation of the first modules. The primary goal of IceCube is the observation of astrophysical neutrinos as a telescope, but it can also be used to study fundamental particle physics properties by measuring atmospheric neutrinos as well as studying cosmic rays.

This chapter first describes the main- and sub-array of the detector and its detection module in Section 1.1, the propagation of particles through ice is explained in Section 1.2, and finally, the signatures that IceCube can observe of the different particles are introduced in Section 1.3.

1.1	Detector Components	1
1.2	Particle Propagation in Ice	4
1.3	Event Morphologies .	7

[1]: Aartsen et al. (2017), “The IceCube Neutrino Observatory: instrumentation and online systems”

1.1 Detector Components

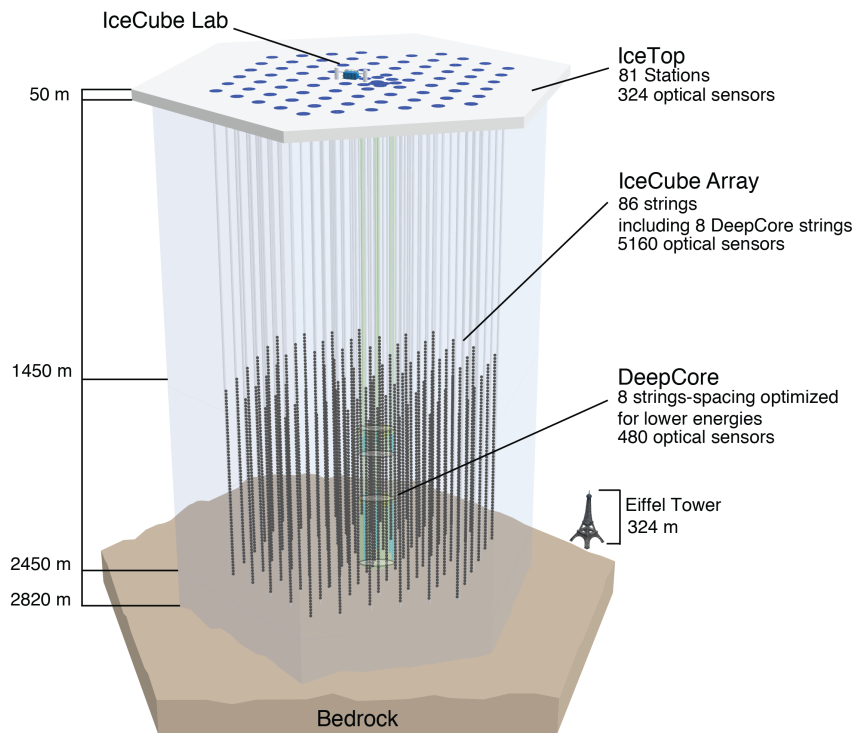


Figure 1.1: Overview of the IceCube detector showing the in-ice main- and sub-array IceCube and DeepCore, IceTop, and the IceCube Laboratory. From [1].

The full IceCube detector array consists of 86 vertical, in-ice strings and 81 surface stations as shown in Figure 1.1. The in-ice part is composed of 60 optical modules per string deployed at depths of 1450 m - 2450 m below the ice, while the surface stations of the cosmic air-shower array, *IceTop*, are ice-filled tanks. The surface stations and the majority of the strings are arranged in a hexagonal grid with the operations building, the *IceCube Laboratory* (ICL), central to the grid on the surface. A top view of the hexagonal arrangement

is shown in Figure 1.4. The in-ice array is designed to detect neutrinos in the energy range from GeV to PeV.

1.1.1 Digital Optical Modules and the Antarctic Ice

The IceCube detection medium is the Antarctic glacial ice itself, which was formed over 100 000 years by accumulation of snow that was subsequently compressed by its own weight to form a dense crystal structure [2]. As a result of this formation process, the optical properties, scattering and absorption, primarily change with depth. Within the detector volume the absorption length ranges from 100 m - 400 m, while the scattering length lies between 20 m and 100 m. They are correlated, with the absorption length being roughly four times the scattering length [3]. The vertical distribution of scattering and absorption length can be seen in Figure 1.2, where one dominant feature is the *dust layer* between 2000 m and 2100 m depth. This region has a higher concentration of dust particles that were deposited in a period of high volcanic activity, which leads to bad optical properties in form of larger scattering and absorption.

[2]: Price et al. (2000), "Age vs depth of glacial ice at South Pole"

SB: there are more properties than just these. Somehow need a half sentence that explains why these are particularly important to single out (see ice papers for inspiration) (ORANGE)

CL: maybe define that absorption and scattering lengths are? they are defined differently so this invites a comparison that is not so obvious (ORANGE)

[3]: Abbasi et al. (2022), "In-situ estimation of ice crystal properties at the South Pole using LED calibration data from the IceCube Neutrino Observatory"

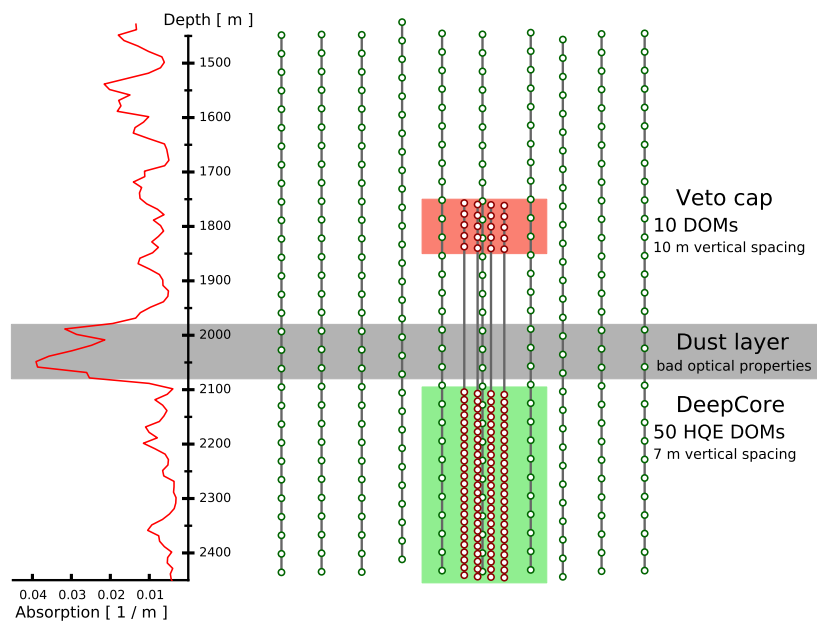
Add reference for the dust layer! Maybe also from the ice paper? mention the dust layer! (ORANGE)

Figure 1.2: A side view of the IceCube and DeepCore showing the depth dependent scattering and absorption length (left panel) and the DOM positions around the dust layer.

exchange for figure with scattering (check abs/sca is correct) (ORANGE)

[4]: Abbasi et al. (2009), "The IceCube data acquisition system: Signal capture, digitization, and timestamping"

[4]: Abbasi et al. (2009), "The IceCube data acquisition system: Signal capture, digitization, and timestamping"



The ice is instrumented by 5160 optical sensors called *digital optical modules* (DOMs) [4], which can detect the Cherenkov light produced by charged particles traveling through the ice. Each DOM is made of a spherical glass housing, containing a downward-facing Photomultiplier Tube (PMT), the main-board with control, readout, and processing-electronics, and a LED flasher-board for calibration purposes. The design and the individual components of a DOM can be seen in Figure 1.3.

The majority of PMTs are the 10" Hamamatsu R7081-02, which have a bialkali photocathode and are sensitive to wavelengths in the range of 300 nm to 650 nm, with a peak quantum efficiency of 25% at 390 nm. In the central part of the IceCube array the peak efficiency reaches 34%. The dark count rate in the temperature range of -40°C to -20°C is ~ 300 Hz. The DOM electronics measure the PMT voltage and control the gain. At a voltage crossing of the equivalent to 0.25 PE the waveform readout is activated [4]. Only when

either one of the nearest or next to nearest DOMs above or below also sees a voltage crossing within a $1\ \mu\text{s}$ time window¹, the voltages are digitized and sent to the ICL. Through the application of a waveform unfolding algorithm, called *WaveDeform* [5], the waveforms are compressed, and the results are the reconstructed times and charges of the photo-electrons. This is the basis for all further IceCube data processing.

The PMT is covered with a mu-metal grid (made from wire mesh), shielding the photocathode from Earth's magnetic field, and it is optically coupled to the glass sphere by RTV silicone gel. The glass sphere is a pressure vessel, designed to withstand both the constant ice pressure and the temporary pressure during the refreezing process of the water in the drill hole during deployment (peaking at around 690 bar). The sphere is held by a harness that connects the DOMs along a string and also guides the cable beside them.

The flasher-board controls 12 LEDs that produce optical pulses with a wavelength of 405 nm [1]. The LEDs can be pulsed separately or in combination with variable output levels and pulse lengths. Using the known information of the light source positions and times this can be used for in-situ calibration of the detector by measuring absorption and scattering properties of the ice. Calibrating the absolute efficiency of the DOMs itself is more accurately done using minimum ionizing muons [6, 7], since the total amplitude of the LED light is not well known.

1.1.2 IceCube Main-Array

The 78 strings that are arranged in a hexagonal pattern from the main part of the in-ice array, which is called *IceCube*. With a $\sim 125\ \text{m}$ horizontal spacing between the strings and a $\sim 17\ \text{m}$ vertical spacing between DOMs, IceCube has a lower energy threshold of around 100 GeV. IceCube was designed to detect astrophysical neutrinos with energies above 1 TeV.

The coordinate system that is used in IceCube is centered at 46500°E , 52200°N at an elevation of 883.9 m [1]. Per definition, it's a right-handed coordinate system where the y-axis points along the Prime Meridian (Grid North) towards Greenwich, UK, and the x-axis points 90° clockwise from the y-axis (Grid East). The z-axis is normal to the ice surface, pointing upwards. For

1: This is referred to as a *hard local coincidence (HLC)* [4].

[5]: Aartsen et al. (2014), "Energy Reconstruction Methods in the IceCube Neutrino Telescope"

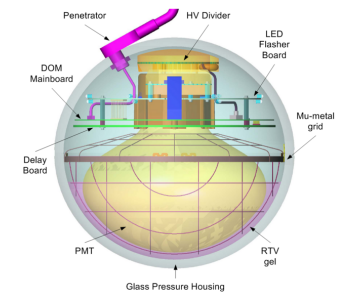


Figure 1.3: Design and components of a digital optical module (DOM) [4]

[1]: Aartsen et al. (2017), "The IceCube Neutrino Observatory: instrumentation and online systems"

[6]: Feintzeig (2014), "Searches for Point-like Sources of Astrophysical Neutrinos with the IceCube Neutrino Observatory"

[7]: Kulacz (2019), "In Situ Measurement of the IceCube DOM Efficiency Factor Using Atmospheric Minimum Ionizing Muons"

Add accuracy of the efficiency calibration here. (ORANGE)

[1]: Aartsen et al. (2017), "The IceCube Neutrino Observatory: instrumentation and online systems"

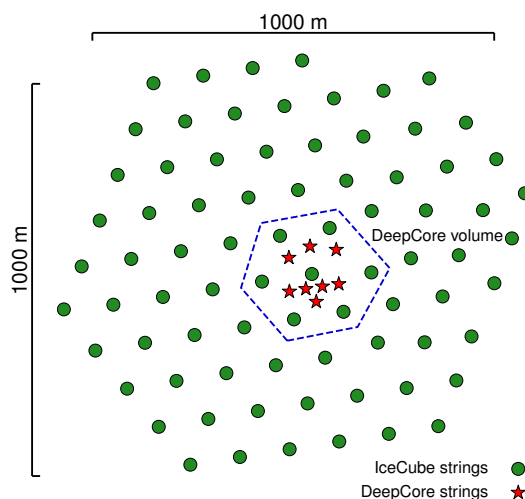


Figure 1.4: Top view of the IceCube array.

IceCube analyses depth is defined as the distance along the z axis from the ice surface, assumed to be at an elevation of 2832 m.

1.1.3 DeepCore Sub-Array

[8]: Abbasi et al. (2012), “The design and performance of IceCube DeepCore”

2: At 400 nm they are 35 % more efficient than the IceCube PMTs [8].

[9]: Abbasi et al. (2023), “Measurement of atmospheric neutrino mixing with improved IceCube DeepCore calibration and data processing”

[10]: Yu et al. (2023), “Recent neutrino oscillation result with the IceCube experiment”

[11]: Cherenkov (1937), “Visible Radiation Produced by Electrons Moving in a Medium with Velocities Exceeding that of Light”

The additional 8 strings form a denser sub-array of IceCube called *DeepCore* [8]. It is located at the bottom-center of the in-ice array and its *fiducial volume* also includes the 7 surrounding IceCube strings as shown in Figure 1.4. The strings in this region have a closer average horizontal distance of about 70 m. The lower 50 DeepCore DOMs on each string are placed in the region of clear ice below the dust layer between 2100 m to 2450 m depth, where their vertical spacing is ~ 7 m. The remaining 10 modules on each string are placed above the dust layer to be used as veto against atmospheric muons as can be seen in Figure 1.2. Additionally, the DeepCore DOMs are equipped with higher quantum efficiency PMTs². The combination of the denser spacing, the high quantum efficiency modules, and the most favorable ice properties below the dust layer leads to a lower energy detection threshold of around 5 GeV, allowing the more efficient observation of atmospheric neutrinos. , which are mostly in the energy range of 10 GeV - 100 GeV. Atmospheric neutrino oscillation analyses result in competitive measurements of the neutrino mixing parameters [9, 10], but the large flux of atmospheric neutrinos allows for many BSM searches, such as searches for dark matter, non-standard interactions, or sterile neutrinos.

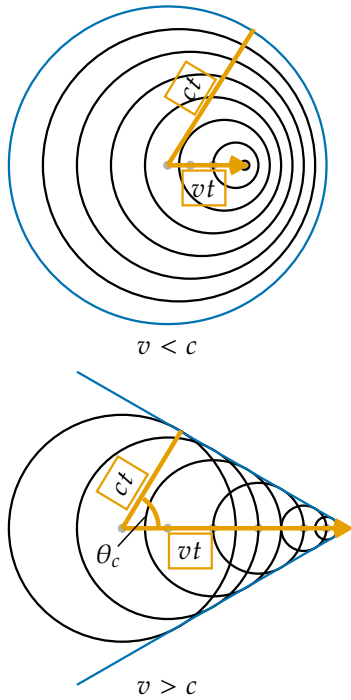


Figure 1.5: Schematic depiction of the spherical light front produced by a particle traveling slower than the speed of light in the medium (top) and the formation of the Cherenkov light front produced by a charged particle traveling faster than the speed of light in the medium (bottom). Blue is the resulting wavefront, while the black circles are spherically emitted light at each position and the orange arrows show the direction of the particle.

1.2 Particle Propagation in Ice

Neutrinos interacting in the ice via DIS produce muons, electromagnetic showers, and hadronic showers, depending on their flavor and the interaction type. The particles produced in those processes mainly lose their energy through *ionization*, *bremsstrahlung*, *pair production*, and the *photo-nuclear interaction*. Electrically charged particles also emit Cherenkov light when traveling through the ice, which is the main observable in IceCube, but only contributes a small amount to the total energy loss. The Cherenkov effect and the energy losses of the particles are described in the following sections, followed by an overview of the different particle signatures in IceCube.

1.2.1 Cherenkov Effect

When a charged particle moves through a medium with a velocity that is greater than the speed of light in that medium, it emits Cherenkov radiation. The detection principle of IceCube DeepCore, is based on the observation of resulting Cherenkov photons that are emitted by the charged secondary particles produced in the neutrino interactions that were introduced in Section ?? . The Cherenkov effect was first observed by Pavel Cherenkov in 1934 [11] and occurs when the charged particle travels faster than the phase velocity of light, therefore polarizing the medium. Upon de-excitation the molecules emit the received energy as photons in a spherical wavefront. Since the particle moves past this wavefront, the superposition of the spherical light emissions forms a cone, which is shown in blue in the bottom panel of Figure 1.5.

Using trigonometry, the angle θ_c at which the Cherenkov light is emitted can be calculated as

$$\theta_c = \arccos\left(\frac{1}{\beta n}\right), \quad (1.1)$$

where β is the velocity of the particle in units of the speed of light and n is the refractive index of the medium. When the particle velocity is close to the speed of light, the equation holds and the angle is only dependent on the refractive index of the medium. For the ice, the refractive index is $n \approx 1.3$ and as a result $\theta_c \approx 41^\circ$ [12].

The frequency of the emission depends on the charge z and the wavelength-dependent index of refraction $n(\omega)$ and is given by the Frank-Tamm formula [13, 14]

$$\frac{d^2N}{dx d\lambda} = \frac{2\pi\alpha z^2}{\lambda^2} \left(1 - \frac{1}{\beta^2 n(\omega)^2}\right), \quad (1.2)$$

with $\alpha \approx 1/137$ the fine structure constant, λ the wavelength of the emitted light, and x the path length traversed by the particle. Relativistic particles in ice produce roughly 250 photons per cm in the wavelength range of 300 nm - 500 nm [15].

1.2.2 Energy Losses

Even though relativistic, charged particles traveling through matter produce Cherenkov radiation, their energy is mainly lost through other processes that are dependent on the particle type and energy. The exact principles of energy loss for the different types can broadly be categorized into the three groups: quasi-continuous energy loss by muons, electromagnetic cascades, and hadronic cascades.

Muons

Muons lose their energy by ionization, bremsstrahlung, pair production, and the photo-nuclear effect. The energy loss by ionization is the dominant process for muons above 1 GeV and has a weak energy dependence given by [16]

$$\left\langle -\frac{dE}{dx} \right\rangle = a_I(E) + b_R(E) \cdot E, \quad (1.3)$$

where E is the energy and $a_I(E)$ and $b_R(E) \cdot E$ are the energy loss by ionization and the combined radiative losses, respectively. In the energy range relevant for this work (10 GeV - 100 GeV), the parameters a_I and b_R only depend on energy very weakly and can be approximated by constants. The energy loss is then given by

$$\left\langle -\frac{dE}{dx} \right\rangle = a + b \cdot E. \quad (1.4)$$

Based on this description, there is a critical energy which divides the regimes where ionization and radiative losses dominate. The critical energy is given by $E_{\text{crit}} = a/b$ and for muons in ice it is ~ 713 GeV (using $a \approx 2.59 \text{ MeVcm}^{-1}$ and $b \approx 3.63 \times 10^{-6} \text{ cm}^{-1}$ [17]). Since the energy range of interest is well below this critical energy, the range of a muon can easily be related to its energy by

$$\langle L \rangle = \frac{E_0}{a}. \quad (1.5)$$

[12]: Petrenko et al. (2002), "214Optical and electronic properties"

[13]: Frank et al. (1937), "Coherent visible radiation from fast electrons passing through matter"

[14]: Tamm (1991), "Radiation Emitted by Uniformly Moving Electrons"

[15]: Radel et al. (2012), "Calculation of the Cherenkov light yield from low energetic secondary particles accompanying high-energy muons in ice and water with Geant4 simulations"

[16]: Workman et al. (2022), "Review of Particle Physics"

[17]: Chirkin et al. (2004), "Propagating leptons through matter with Muon Monte Carlo (MMC)"

Measuring the length of a muon track therefore allows for an estimation of its energy if the full track is contained within the instrumented volume of IceCube. Using the given numbers a 30 GeV muon travels ~116 m, which is well within the instrumented volume of IceCube, which spans across distances of up to 1000 m. This approximate treatment does not take into account the stochastic nature of some energy losses. Bremsstrahlung and photo-nuclear interactions for example rarely occur, but when they do, they deposit a large chunk of energy. A thorough investigation of the energy losses of muons in ice can be found in [18].

[18]: Raedel (2012), "Simulation Studies of the Cherenkov Light Yield from Relativistic Particles in High-Energy Neutrino Telescopes with Geant4"

Electromagnetic Showers

Photons as well as electrons and positrons are produced either directly in neutrino interactions or in secondary particle interactions. Above a critical energy E_c , they lose their energy through repeated pair production and bremsstrahlung emission forming an expanding, electromagnetic shower profile. The particles' energy reduces with every interaction and their number increases until they fall below the critical energy where ionization and excitation of surrounding atoms become the dominant energy loss processes for electrons and positrons. For photons the remaining energy is lost through the Compton effect and the photoelectric effect [16]. Below the critical energy no new shower particles are produced. Electromagnetic cascades can be characterized by the radiation length, X_0 , after which electrons/positrons reduced their energy to $1/e$ of their initial energy. For photons, it's equivalent to $7/9$ of the mean free path of pair production. The critical energy for ice is $E_c \approx 78$ MeV, with a radiation length of $X_0 \approx 39.3$ cm [19].

[16]: Workman et al. (2022), "Review of Particle Physics"

[19]: Tanabashi et al. (2018), "Review of Particle Physics"

The radiation length governs the longitudinal shower profile and using $t = x/X_0$, the shower intensity can be described by a gamma distribution [16, 20]

$$\frac{dE}{dt} = E_0 b \frac{(bt)^{a-1} e^{-bt}}{\Gamma(a)}, \quad (1.6)$$

where a and b are parameters that have to be estimated from experiment, and E_0 is the initial shower energy. Based on the work from [18], performed with GEANT4 [21], the parameters for electromagnetic showers in ice are

$$e^- : a \approx 2.01 + 1.45 \log_{10}(E_0/\text{GeV}), b \approx 0.63, \quad (1.7a)$$

$$e^+ : a \approx 2.00 + 1.46 \log_{10}(E_0/\text{GeV}), b \approx 0.63, \quad (1.7b)$$

$$\gamma : a \approx 2.84 + 1.34 \log_{10}(E_0/\text{GeV}), b \approx 0.65. \quad (1.7c)$$

The maximum of the shower is at $t_{max} = (a - 1)/b$ and the Cherenkov emission of the charged particles produced in the shower is peaked around the Cherenkov angle, since they are produced in the forward direction.

Add angular profile plot (Summer agrees!) (create one based on Leif R  del as Alex did) (RED)

Hadronic Showers

In DIS interactions, a cascade is always produced by the hadrons coming from the breaking target nucleus. The cascade is a result of secondary particles produced in strong interactions between the hadrons and the traversed matter. The charged particles produced in the shower will emit Cherenkov radiation, while neutral particles will be invisible to the detector. There is also an electromagnetic component of the shower, due to for example the

decay of neutral pions into photons. Hadronic showers of the same energy as electromagnetic showers have larger fluctuations in energy deposition and shape, since they depend on the produced particle types. Hadrons also have a higher energy threshold for Cherenkov light production, because of their higher mass. Based on [18, 22], the visible electromagnetic fraction of hadronic showers can be parameterized as

$$F(E_0) = \frac{T_{\text{hadron}}}{T_{\text{EM}}} = 1 - (1 - f_0) \left(\frac{E_0}{E_s} \right)^{-m}, \quad (1.8)$$

where $T_{\text{hadron/EM}}$ is the total track length of a hadronic/electromagnetic shower with the same energy, f_0 is the ratio of hadronic and electromagnetic light yield, E_0 is the initial energy, and E_s is an energy scale. The parameter m is a free model parameter. The ratio $F(E_0)$ increases with energy, but is always smaller than 1. The variance of this distribution is given by

$$\sigma_F(E_0) = \sigma_0 \log(E_0)^{-\gamma}. \quad (1.9)$$

The parameters m , E_s , and f_0 were estimated by fitting the model to the results of Geant4 simulations. Cherenkov light from hadronic showers also peaks around the Cherenkov angle, but the angular distribution is more smeared out, due to the variations in particle type and their energy depositions.

[18]: Raedel (2012), “Simulation Studies of the Cherenkov Light Yield from Relativistic Particles in High-Energy Neutrino Telescopes with Geant4”

[22]: Gabriel et al. (1994), “Energy dependence of hadronic activity”

1.3 Event Morphologies

The event morphologies produced by particles detected in IceCube are combinations of the three energy loss types described in Section 1.2.2, e.g. *cascades* from electromagnetic and hadronic showers and elongated *tracks* from muons traveling through the detector. Table 1.1 gives an overview of the possible event signatures.


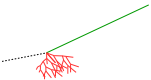

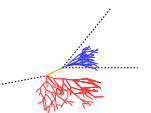
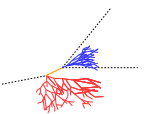
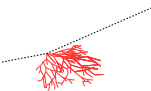
Neutrino interactions are observed as cascades, tracks, or a combination of both, depending on the initial flavor and the interaction type for the specific event.

In ν_μ - CC interactions, a muon is produced in addition to a hadronic shower from the breaking nucleus. If the interaction happens outside the detector, but the muon passes through the detector, this will create a track-like signature. The same happens if the interaction happens inside, but the energy transfer to the nucleus is small ($y \approx 0$). At energies relevant for this work, tracks have length at the same order of the distance between DOMs, so they can be observed as such.

If the interaction happens inside the detector and the energy transfer to the hadronic part of the shower is larger, it will create a cascade with a track leaving it. A similar signature is observed after a ν_τ - CC interaction, in which a tau is produced that later decays into a muon, with a branching ratio of 17 %. In those cases the muon usually has a lower energy and the track will be fainter and harder to observe.

The other 83 % of ν_τ - CC interactions produce a tau that decays into an electron or hadrons, leaving a cascade-only signature through the electromagnetic or hadronic shower. All ν_e - CC interactions also produce pure

Table 1.1: IceCube low energy event signatures, their underlying interaction type, and the particles that produce them. Also shown are the secondary particles produced in the interactions. Black dashed lines represent neutrinos, green lines muons, orange line leptons, and blue and red lines are particles in electromagnetic and hadronic cascades, respectively. Adapted from [23].

Interaction	Secondary particles	Signature
$\text{CC } \nu_\mu^{(-)}$		μ^\pm track
		μ^\pm track and hadrons
$\text{CC } \nu_\tau^{(-)}$		τ^\pm decaying into μ^\pm ($\sim 17\%$ BR), hadrons
		τ^\pm decaying into e^\pm or hadrons ($\sim 83\%$ BR)
$\text{CC } \nu_e^{(-)}$		e^\pm , hadrons
$\text{NC } \nu_\ell^{(-)}$		hadrons

cascades, since the electron quickly loses its energy in an electromagnetic shower. In all ν - NC interactions, the produced neutrino escapes and only the hadronic shower is observable. Since the size of the cascades at the energy range of interest is smaller than the spacing of the DOMs, they are approximately observed as point-like, spherical light sources. Even though the light is almost isotropically emitted, some asymmetry remains in the light profile, which can be used to reconstruct the direction of the incoming neutrino.

Atmospheric muons also produce pure track like signatures, similar to ν_μ - CC interactions happening outside the detector. They are one of the main backgrounds for analyses using atmospheric neutrinos and are therefore the target of many filter steps described in Section ??.

Search for Tau Neutrino Induced Heavy Neutral Lepton Events

2

This chapter describes the search for HNL events using 10 years of IceCube DeepCore data. The expected number of HNL events in the data sample depends on the mass of the additional heavy state, m_4 , and the mixing element $|U_{\alpha 4}^2|$, with $\alpha = e, \mu, \tau$, between the SM flavors and the new mass state. As discussed in Section ??, this work focuses on the mixing to the tau sector, $|U_{\tau 4}^2|$, which has the weakest constraints to date. Since the mass itself influences the production and decay kinematics of the event and the accessible decay modes, individual mass samples were produced as described in Section ?. The mass influences the decay length and energy distributions, while the mixing both changes the overall expected rate of the HNL events and the shape in energy and length. We perform three independent searches for each mass sample, where the mixing is measured in each of the fits.

2.1	Final Level Sample	9
2.2	Statistical Analysis	12
2.3	Analysis Checks	16
2.4	Results	18
2.5	Outlook	21

2.1 Final Level Sample

The final level simulation sample of this analysis consists of the neutrino and muon MC introduced in Section ?? and one of the three HNL samples explained in Section ??, while the data are the events measured in 10 years of IceCube DeepCore data taking. All simulation and the data are processed through the full event selection chain described in Section ?? and Section ?? leading to the final level sample. As described in Section ??, event triggers consisting purely of random coincidences induced by noise in the DOMs have been reduced to a negligible rate, and will not be discussed further.

To get the neutrino expectation, the MC events are weighted according to their generation weight introduced in Section ??, multiplied by the total lifetime, and the expected neutrino flux. For the correct expectation at the detector, the events have to be weighted by the oscillation probability, depending on their energy and their distance traveled from the atmosphere to the detector. The oscillation probabilities are calculated using a PYTHON implementation of the calculations from [24], which use the matter profile of the Earth following the *Preliminary Reference Earth Model (PREM)* [25] as input. Apart from the energy and the distance, the two relevant parameters defining the oscillation probabilities are the atmospheric neutrino oscillation parameters θ_{23} and Δm_{31}^2 . Since the HNL events originate from the tau neutrinos that were produced as muon neutrinos in the atmosphere and then oscillated into ν_τ , this weighting is also applied in addition to the specific weighting scheme for the HNL events described in Section ??, which itself is defined by the mixing $|U_{\tau 4}^2|$ and the mass m_4 .

[24]: Barger et al. (1980), “Matter effects on three-neutrino oscillations”

[25]: Dziewonski et al. (1981), “Preliminary reference Earth model”

2.1.1 Expected Rates/Events

The rates and the expected number of events for the SM background are shown in Table 2.1 with around 175000 total events expected in the 10 years. Only data marked as good is used for the analysis, where *good* refers to

measurement time with the correct physics run configuration and without other known issues. The resulting good detector livetime in this data taking period was 9.28 years. The rates are calculated by summing the weights of all events in the final level sample, while the uncertainties are calculated by taking the square root of the sum of the weights squared. The expected number of events is calculated by multiplying the rate with the livetime. The individual fractions show that this sample is neutrino dominated where the majority of events are ν_μ -CC events.

Table 2.1: Final level rates and event expectation of the SM background particle types.

Type	Rate [mHz]	Events (9.28 years)	Fraction [%]
ν_μ^{CC}	0.3531	103321 ± 113	58.9
ν_e^{CC}	0.1418	41490 ± 69	23.7
ν_τ^{NC}	0.0666	19491 ± 47	11.1
ν_τ^{CC}	0.0345	10094 ± 22	5.8
μ_{atm}	0.0032	936 ± 15	0.5
total	0.5992	175332 ± 143	100.0

Table 2.2 shows the rates and expected number of events for the HNL signal simulation. The expectation depends on the mass and the mixing and shown here are two example mixings for all the three masses that are being tested in this work. A mixing of 0.0 would result in no HNL events at all. It can already be seen that for the smaller mixing of $|U_{\tau 4}|^2 = 10^{-3}$ the expected number of events is very low, while at the larger mixing of $|U_{\tau 4}|^2 = 10^{-1}$ the number is comparable to the amount of atmospheric muons in the background sample.

Table 2.2: Final level rates and event expectations of the HNL signal for all three masses and two example mixing values.

HNL mass	Rate [μHz]	Events (in 9.28 years)
$ U_{\tau 4} ^2 = 10^{-1}$		
0.3 GeV	3.3	975 ± 2
0.6 GeV	3.1	895 ± 2
1.0 GeV	2.5	731 ± 2
$ U_{\tau 4} ^2 = 10^{-3}$		
0.3 GeV	0.006	1.67 ± 0.01
0.6 GeV	0.022	6.44 ± 0.01
1.0 GeV	0.025	7.27 ± 0.01

2.1.2 Analysis Binning

[10]: Yu et al. (2023), “Recent neutrino oscillation result with the Ice-Cube experiment”

An identical binning to the analysis performed in [10] is used. In total, there are three bins in PID (cascade like, mixed, and track like), 12 bins in reconstructed energy, and 8 bins in cosine of the reconstructed zenith angle as specified in Table 2.3. Extending the binning towards lower energies or

Add fractions of the different particle types in the bins for benchmark mass/mixing (another table?) (ORANGE)

Variable	N_{bins}	Edges	Spacing
P_ν	3	[0.00, 0.25, 0.55, 1.00]	linear
E	12	[5.00, 100.00]	logarithmic
$\cos(\theta)$	8	[-1.00, 0.04]	linear

increasing the number of bins in energy or cosine of the zenith angle did not improve the HNL sensitivities significantly, because the dominant signal region is already covered with a sufficiently fine binning to observe the shape and magnitude of the HNL events on top of the SM background. This

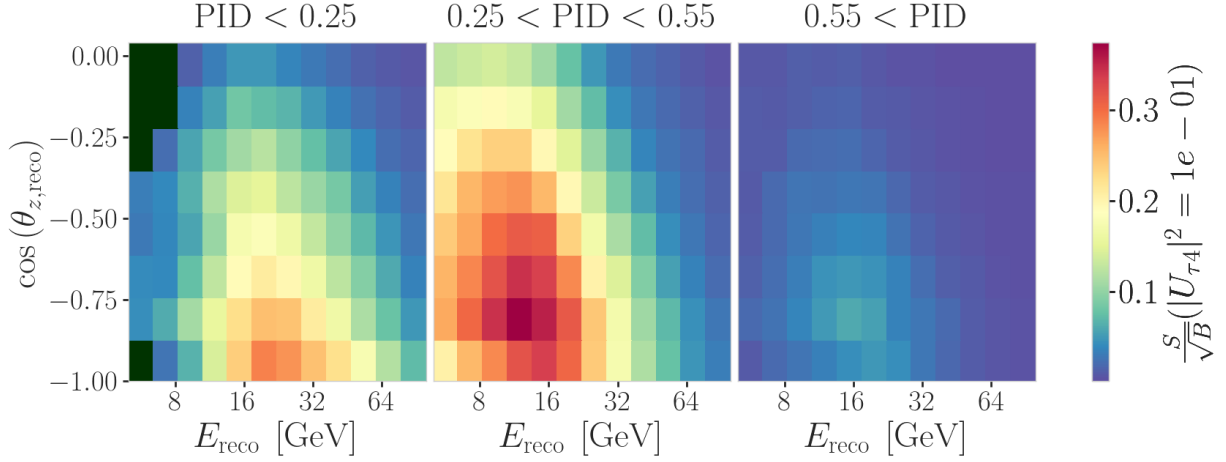


Figure 2.1: Signal over square root of background expectation in 9.28 years for the 1.0 GeV mass sample at a mixing of 0.1, while all other parameters are at their nominal values.

can be seen in the middle panel of Figure 2.1, which shows the expected signal events divided by the square root of the expected background events for every bin used in the analysis. The signal expectation is using the 1.0 GeV mass sample at a reference mixing of 0.1, with the corresponding three dimensional histogram shown in Figure ?? . Both the nominal background expectation used to calculate the signal to square root of background ratio and the detector data can be seen in Figure 2.2.

Some low energy bins in the cascade like region have very low MC expectations (<1 event) and are therefore not taken into account in the analysis, to prevent unwanted behavior in the fit. Those are shown in dark green in the three dimensional histograms, and both background and data histograms show a strong decrease of events towards low energies in the cascade like bin. This background expectation is not necessarily supposed to agree with the data, because this is the distributions assuming nominal parameter values, before performing the fit to find the parameters that describe the data best. All parameters used in the analysis are discussed in Section 2.2.2, and post-fit data to MC comparisons are shown in Section 2.3.3.

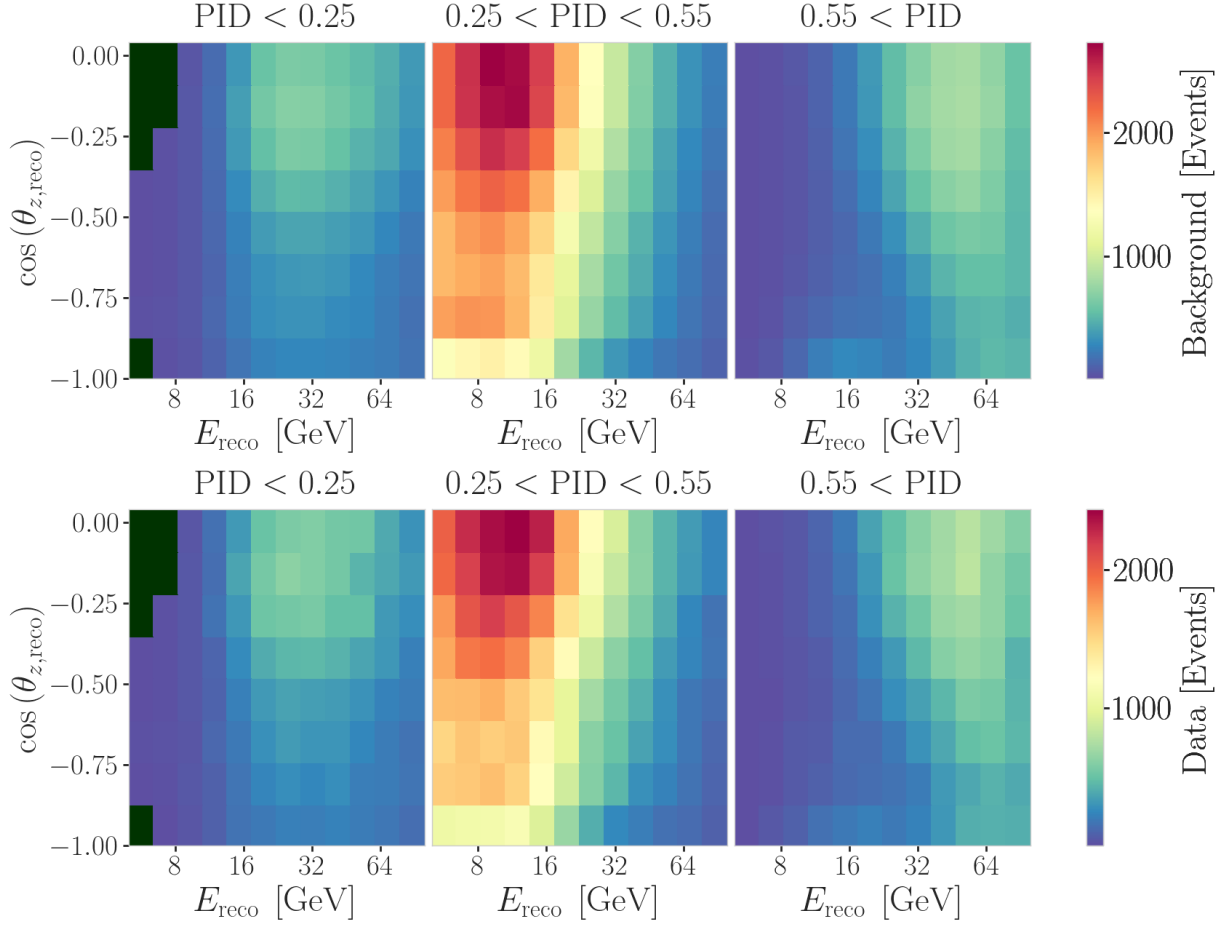


Figure 2.2: Background expectation in 9.28 years for all other parameters are at their nominal values (top) and observed data (bottom).

2.2 Statistical Analysis

2.2.1 Test Statistic

The measurements are performed by comparing the weighted MC to the data. Through variation of the nuisance and physics parameters that govern the weights, the best matching set of parameters can be found, by optimizing a fit metric. The comparison is done using a modified χ^2 , defined as

$$\chi_{\text{mod}}^2 = \sum_{i \in \text{bins}} \frac{(N_i^{\text{exp}} - N_i^{\text{obs}})^2}{N_i^{\text{exp}} + (\sigma_i^{\nu})^2 + (\sigma_i^{\mu})^2 + (\sigma_i^{\text{HNL}})^2} + \sum_{j \in \text{syst}} \frac{(s_j - \hat{s}_j)^2}{\sigma_{s_j}^2}, \quad (2.1)$$

as the fit metric. It is designed such that taking the difference between a free fit and a fit with fixed parameters based on a chosen hypothesis, $\Delta\chi_{\text{mod}}^2$, can directly be used as a *test statistic* (*TS*) for hypothesis testing, due to its asymptotic behavior. The total even expectation is $N_i^{\text{exp}} = N_i^{\nu} + N_i^{\mu} + N_i^{\text{HNL}}$, where N_i^{ν} , N_i^{μ} , and N_i^{HNL} are the expected number of events in bin i from neutrinos, atmospheric muons, and HNLs, while N_i^{obs} is the observed number of events in the bin. The expected number of events from each particle type is calculated by summing the weights of all events in the bin $N_i^{\text{type}} = \sum_i^{\text{type}} \omega_i$, with the statistical uncertainty being $(\sigma_i^{\text{type}})^2 = \sum_i^{\text{type}} \omega_i^2$. The additional term in Equation 2.1 is included to apply a penalty term for

prior knowledge of the systematic uncertainties of the parameters where they are known. s_j are the systematic parameters that are varied in the fit, while \hat{s}_j are their nominal values and σ_{s_j} are the known uncertainties.

2.2.2 Physics Parameters

The variable physics parameter in this analysis is the mixing between the HNL and the SM τ sector, $|U_{\tau 4}|^2$. It is varied continuously in the range of $[0.0, 1.0]$ by applying the weighting scheme described in Section ?? . The fit is initialized at an off-nominal value of 0.1. The other physics parameter, the mass m_4 of the HNL, is implicitly fixed to one of the three discrete masses to be tested, by using the corresponding sample of the HNL simulation described in Section ?? .

2.2.3 Nuisance Parameters

All systematic parameters introduced in Section ?? apart from the detector calibration uncertainties, are already parameterized in a continuous way and can be varied in the fit. To be able to do the same with the detector uncertainties, a novel method is applied that will briefly be introduced here before going into the selection of the free parameters.

Treatment of Detector Systematic Uncertainties

Since the variations related to the detector calibration uncertainties introduced in Section ?? are estimated by simulating MC at discrete values of the systematic parameters, a method to derive continuous variations is needed to perform the fit. The method applied here was initially introduced in [26] and first used in the low energy sterile neutrino search in [27] (section 7.4.3). Using a *likelihood-free inference* technique, re-weighting factors are found for every event in the nominal MC sample, given a specific choice of detector systematic parameters. These factors quantify how much more or less likely the event would be for the corresponding change in detector response from the nominal parameters. Without going into the details of the method, which were already exhaustively discussed in [26] and [27], the performance is assessed here for the HNL signal simulation. In order to do so, the weights are applied to the nominal MC samples, choosing the detector systematic values used to produce the discrete samples and the resulting event expectations are compared to the expectations from the individual, discrete MC samples. The bin counts are compared by calculating the pull defined as

$$p = \frac{N_{\text{reweighted}} - N_{\text{sys}}}{\sqrt{\sigma_{\text{reweighted}}^2 + \sigma_{\text{sys}}^2}}, \quad (2.2)$$

where N are the bin-wise event expectations and σ are their MC uncertainty. For the SM BG simulation, the performance was already investigated in [28] (section 7.4.4, appendix B5) and the re-weighted nominal MC was shown to be in agreement with the discrete systematic sets at a sufficient level. Figure ?? shows the bin-wise pulls for the 1.0 GeV HNL mass sample at a mixing of 0.1 for a selection of the discrete systematic samples, where the DOM efficiency and the bulk ice absorption was varied by $\pm 10\%$. As expected,

[26]: Fischer et al. (2023), “Treating detector systematics via a likelihood free inference method”

[27]: Trettin (2023), “Search for eV-scale sterile neutrinos with IceCube DeepCore”

[28]: Lohfink (2023), “Testing non-standard neutrino interaction parameters with IceCube-DeepCore”

the pull distributions follow a standard normal distribution, without strong clustering or any systematic deviations. A similar performance is found for the additional systematic variations and the detailed figures can be found in Section ??.

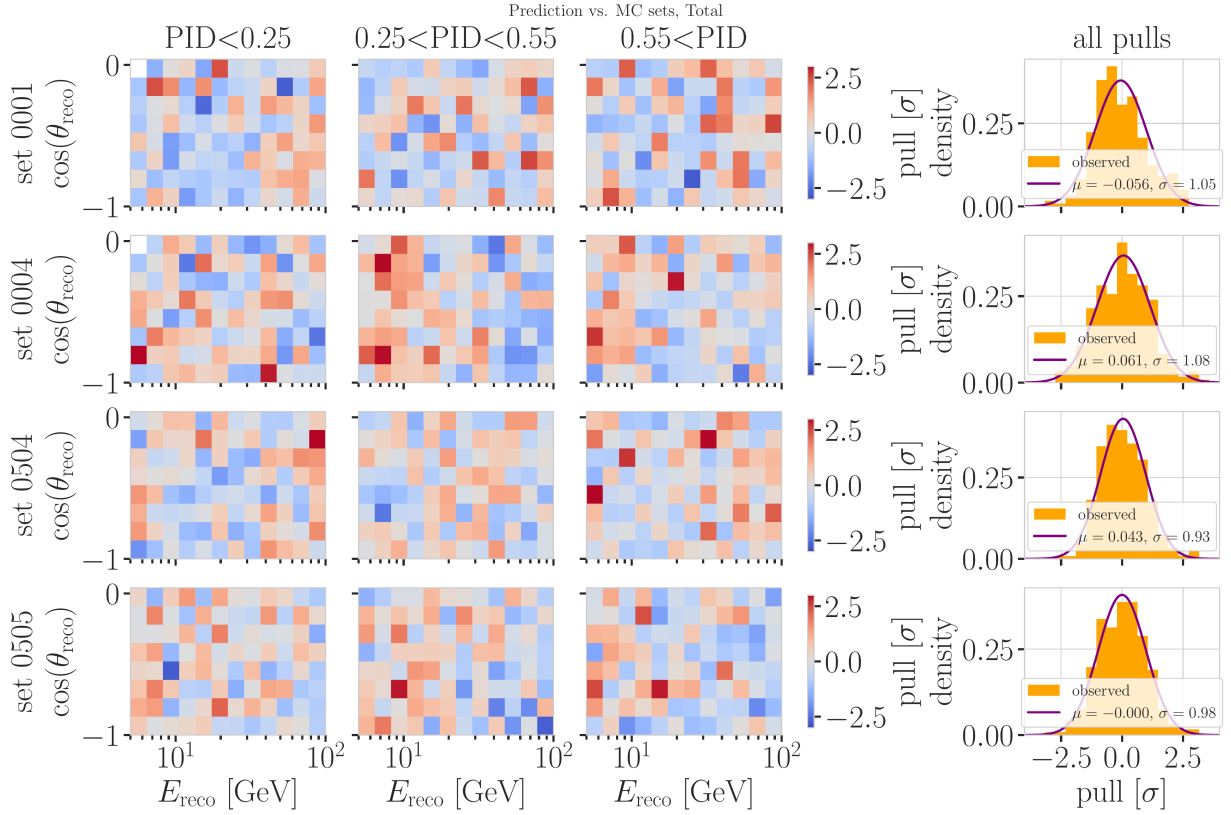


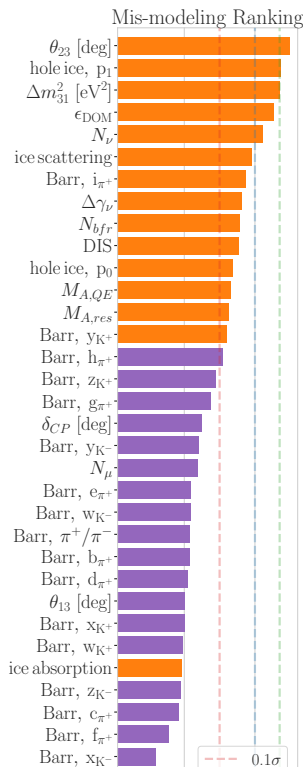
Figure 2.3: Three dimensional pulls and set-wise pull distributions between the nominal set and the specific systematic sets, after the nominal set was re-weighted to the corresponding systematic parameter value.

fix caption (add description of what specific set number means (RED))

Free Parameters

To decide which systematic uncertainties should be included in the fit, we test the potential impact they have on the TS if they are neglected. The test is performed by creating Asimov data using the BG simulation and the HNL simulation of the 1.0 GeV mass sample at a mixing value of 0.1, which is chosen as a benchmark physics parameter, but the explicit choice does not have a significant impact on the test. The systematic parameter of interest is set to a value above its nominal expectation, either pulled up by $+1\sigma$ or by an educated estimate for parameters without a well-defined uncertainty. A fit is performed fixing the systematic parameter of interest and leaving all additional parameters free. The resulting TS is the fit metric difference between between this fit and a fit with all parameters free, which would result in a fit metric of 0.0 for this Asimov test. This difference is called mis-modeling significance and parameters below a significance of 0.1σ are fixed. The test is performed in an iterative manner until the final set of free parameters is found.

Figure 2.4 shows the resulting significances of one of these tests. The parameters tested are the systematic parameters introduced in Section ?? and the atmospheric oscillation parameters mentioned in Section 2.1. In the



final selection of free parameters the Barr h_{π^+} parameter was also left free, to sufficiently cover the relevant energy production range of the Pions, as can be seen in Figure ??, where both for Kaons and Pions the uncertainties are included for primary energies above 30 GeV and $x_{\text{lab}} > 0.1$. Additionally, the ice absorption is still kept free, despite showing a small significance, which is done because the bulk ice parameters are not well constrained and are known to have a large impact, which might be concealed in this idealized test, due to correlations with the other parameters. In this test, the effect of correlations is challenging to consider, because only the impact of one parameter is tested at a time, using the overall mis-modeling significance as a measure. The mis-modeling could be reduced by a correlated parameter capturing the effect of the parameter of interest. For this reason a very conservative threshold of 0.1σ is chosen and some parameters below the threshold are still left free in the fit.

All nuisance parameters that are left free in the fit are summarized in Table 2.4, showing their nominal values, the allowed fit ranges, and their Gaussian prior, if applicable. The scaling parameter N_ν is included to account for the overall normalization of the neutrino rate, and it has the identical effect on the SM neutrino events and the BSM HNL events, because they both originate from the same neutrino flux. Despite being known to $\sim 5\%$ in this energy range, there is no prior applied to this parameter, because the fit itself is able to constrain it well, which can be seen by the large impact it shows in Figure 2.4. Concerning the atmospheric neutrino flux, the CR power law flux correction factor $\Delta\gamma_\nu$ introduced in Section ?? is included with nominal value of 0.0 which corresponds to the baseline flux model by Honda *et al* [29]. A slightly conservative prior of 0.1 is applied to the parameter, while latest measurements show an uncertainty of 0.05 [30]. The Barr parameters are constrained by a Gaussian prior, taken from [31]. All the detector systematic uncertainties discussed in Section ?? are included in the fit. The DOM efficiency ϵ_{DOM} is constrained by a Gaussian prior with a width of 0.1, which is a conservative estimate based on the studies of the optical efficiency using minimum ionizing muons from [6, 7]. The two atmospheric neutrino oscillation parameters θ_{23} and Δm_{31}^2 are also included in the fit with nominal values of 47.5° and $2.48 \times 10^{-3} \text{ eV}^2$ [10], respectively. Since they govern the shape and the strength of the tau neutrino flux, by defining the oscillation from ν_μ to ν_τ , they are also relevant for the HNL signal shape.

Need cite here! (RED)

[29]: Honda et al. (2015), "Atmospheric neutrino flux calculation using the NRLMSISE-00 atmospheric model"

[30]: Evans et al. (2017), "Uncertainties in atmospheric muon-neutrino fluxes arising from cosmic-ray primaries"

[31]: Barr et al. (2006), "Uncertainties in Atmospheric Neutrino Fluxes"

[6]: Feintzeig (2014), "Searches for Point-like Sources of Astrophysical Neutrinos with the IceCube Neutrino Observatory"

[7]: Kulacz (2019), "In Situ Measurement of the IceCube DOM Efficiency Factor Using Atmospheric Minimum Ionizing Muons"

[10]: Yu et al. (2023), "Recent neutrino oscillation result with the IceCube experiment"

2.2.4 Low Energy Analysis Framework

The analysis is performed using the PISA [32] [33] software framework, which was developed to perform analyses of small signals in high-statistics neutrino oscillation experiments. It is used to generate the expected event distributions from several MC samples, which can then be compared to the observed data. The expectation for each MC sample is calculated by applying physics and nuisance parameter effects in a stage-wise manner, before combining them to the final expectation.

I could add some final level effects of some systematics on the 3D binning and maybe discuss how they are different from the signal shape, or so? (ORANGE)

[32]: Aartsen et al. (2020), "Computational techniques for the analysis of small signals in high-statistics neutrino oscillation experiments"

Table 2.4: Systematic uncertainty parameters that are left free to float in the fit. Their allowed fit ranges are shown with the nominal value and the Gaussian prior width if applicable.

Parameter	Nominal	Range	Prior
$\theta_{23} [^\circ]$	47.5047	[0.0, 90.0]	-
$\Delta m_{31}^2 [\text{eV}^2]$	0.002475	[0.001, 0.004]	-
N_ν	1.0	[0.1, 2.0]	-
$\Delta \gamma_\nu$	0.0	[-0.5, 0.5]	0.1
Barr h_{π^+}	0.0	[-0.75, 0.75]	0.15
Barr i_{π^+}	0.0	[-3.05, 3.05]	0.61
Barr y_{K^+}	0.0	[-1.5, 1.5]	0.3
DIS	0.0	[-0.5, 1.5]	1.0
$M_{A,QE}$	0.0	[-2.0, 2.0]	1.0
$M_{A,res}$	0.0	[-2.0, 2.0]	1.0
ϵ_{DOM}	1.0	[0.8, 1.2]	0.1
hole ice p_0	0.101569	[-0.6, 0.5]	-
hole ice p_1	-0.049344	[-0.2, 0.2]	-
bulk ice absorption	1.0	[0.85, 1.15]	-
bulk ice scattering	1.05	[0.9, 1.2]	-
N_{bfr}	0.0	[-0.2, 1.2]	-

2.3 Analysis Checks

Fitting to data is performed in a *blind* manner, where the analyzer does not immediately see the fitted physics and nuisance parameter values, but first checks that a set of pre-defined *goodness of fit* (GOF) criteria are fulfilled. This is done to circumvent the so-called *confirmation bias* [34], where the analyzer might be tempted to construct the analysis in a way that confirms their expectation. After the GOF criteria are met to satisfaction, the fit results are unblinded and the full result can be revealed. Before these blind fits to data are performed, the robustness of the analysis method is tested using pseudo-data that is generated from the MC.

[34]: Nickerson (1998), “Confirmation Bias: A Ubiquitous Phenomenon in Many Guises”

1: There is a degeneracy between the lower octant ($\theta_{23} < 45^\circ$) and the upper octant ($\theta_{23} > 45^\circ$), which can lead to fit metric minima (local and global) at two positions that are mirrored around 45° in θ_{23} .

[35]: Dembinski et al. (2022), *scikit-hep/iminuit: v2.17.0*

[36]: James et al. (1975), “Minuit: A System for Function Minimization and Analysis of the Parameter Errors and Correlations”

Fit	Err.	Prec.	Tol.
Coarse	1e-1	1e-8	1e-1
Fine	1e-5	1e-14	1e-5

Table 2.5: Migrad settings for the two stages in the minimization routine. *Err.* are the step size for the numerical gradient estimation, *Prec.* is the precision with which the LLH is calculated, and *Tol.* is the tolerance for the minimization.

Find first occurrence of "Asimov" and add reference and explain it there (RED)

2: A pseudo-data set without statistical fluctuations is called Asimov data set.

2.3.1 Minimization Robustness

To find the set of parameters that best describes the data, a staged minimization routine is used. In the first stage, a fit with coarse minimizer settings is performed to find a rough estimate of the *best fit point* (BFP). In the second stage, the fit is performed again in both octants¹ of θ_{23} , starting from the BFP of the coarse fit. For each individual fit the *MIGRAD* routine of *iminuit* [35] is used to minimize the χ_{mod}^2 fit metric defined in Equation 2.1. *iminuit* is a fast, python compatible minimizer based on the *MINUIT2* C++ library [36]. The individual minimizer settings for both stages are shown in Table 2.5.

To test the minimization routine and to make sure it consistently recovers any physics parameters, pseudo-data sets are produced from the MC by choosing the nominal nuisance parameters and specific physics parameters, without adding any statistical or systematic fluctuations to it. These so-called *Asimov*² data sets are then fit back with the full analysis chain. This type of test is called *Asimov inject/recover test*. A set of mixing values between 10^{-3} and 10^0 is injected and fit back. Without fluctuations the fit is expected to always recover the injected parameters (both physics and nuisance parameters). The fitted mixing values from the *Asimov inject/recover tests* are compared to the true injected values in Figure 2.5 for all three mass samples. As desired, the fit is always able to recover the injected physics parameter and the

nuisance parameters within the statistical uncertainty or at an insignificant fit metric difference.

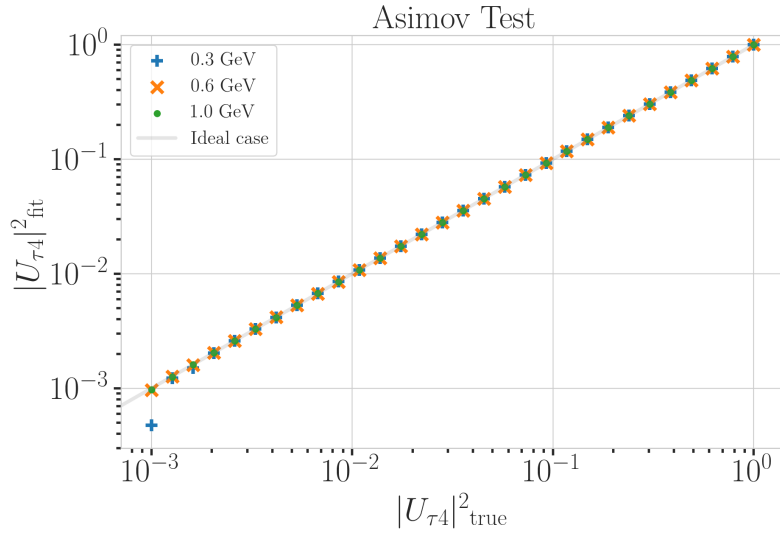


Figure 2.5: Asimov inject/recover test results for all three mass samples. Mixing values between 10^{-3} and 10^0 are injected and fit back with the full analysis chain. The injected parameter is always recovered within the statistical uncertainty or at an insignificant fit metric difference.

2.3.2 Goodness of Fit

To estimate the GOF, pseudo-data is generated from the MC by injecting the BFP parameters as true parameters and then fluctuating the expected bin counts to account for MC uncertainty and Poisson fluctuations in data. First, the expectation value of each bin is drawn from a Gaussian distribution centered at the nominal expectation value with a standard deviation corresponding to the MC uncertainty of the bin. Based on this sampled expectation value, each bin count is drawn from a Poisson distribution, independently, to get the final pseudo-data set. These pseudo-data sets are analyzed with the same analysis chain as the real data, resulting in a final fit metric value for each pseudo-data set. By comparing the distribution of fit metric values from this *ensemble* of pseudo-data trials to the fit metric of the fit to real data, a p-value can be calculated. The p-value is the probability of finding a value of the fit metric at least as large as the one from the data fit. Figure 2.6 shows the distribution from the ensemble tests for the 0.6 GeV mass sample and the observed value from the fit, resulting in a p-value of 28.5 %. The p-values for the 0.3 GeV and 1.0 GeV are 28.3 % and 26.0 %, respectively, and the corresponding plots are shown in Section ?? . Based on this test, it is concluded that the fit result is compatible with the expectation from the ensemble of pseudo-data trials.

2.3.3 Data/MC Agreement

At the BFP, the agreement between the data and simulation is probed by comparing both the one dimensional analysis distributions for PID, energy, and cosine of the zenith angle as well as the full three dimensional distributions. Figure 2.7 shows the three dimensional pull distribution between data and the total MC expectation for the 0.6 GeV mass sample at the BFP. The pulls are evenly spaced and show no strong clustering. In

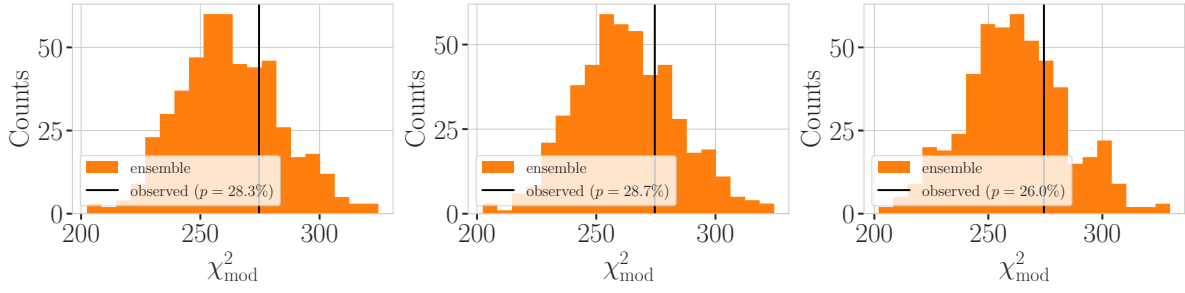


Figure 2.6: Observed fit metric (data fit) and fit metric distribution from pseudo-data ensemble generated around the best fit point. Shown are the results for all three mass samples, with the ensemble distribution on orange, the observed value in black, and the p-value in the legend.

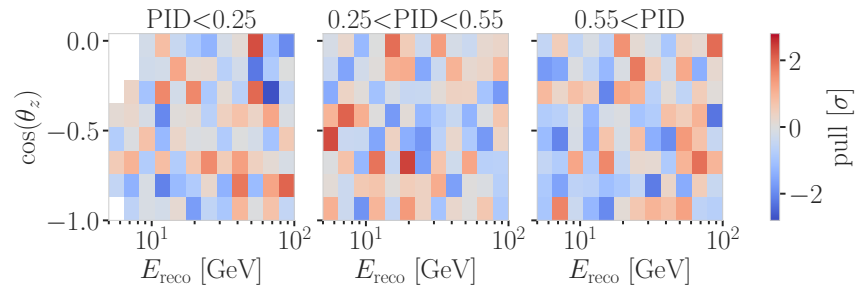
Figure ??, two examples of the one dimensional distributions for the energy and cosine of the zenith angle are shown for the 0.6 GeV mass sample. The data is compared to the total MC expectation, which is also split up into the individual signal and background components for illustration. Good agreement can be observed in the pull distributions, and is quantified by a reduced χ^2 , which is close to 1.0 for all distributions. The reduced χ^2 for all investigated distributions is listed in Table ??, while the distributions themselves can be found in Section ??.

add 1-d data/mc agreement for example mass sample (0.6?) and all 3 analysis variables (RED)

add table with reduced chi2 for all 1-d distributions (RED)

Figure 2.7

fix caption and describe plot in text (RED)



2.4 Results

2.4.1 Best Fit Nuisance Parameters

The resulting nuisance parameter values from the fits are illustrated in Figure 2.8, where the differences to the nominal values are shown, normalized by the distance to the closest boundary. The results from all three fits are shown in the same plot and the fits prefer values of the same size for all three mass samples. For parameters that have a Gaussian prior, the 1σ range is also displayed. As was already confirmed during the blind fit procedure, all fitted parameters are within this range. The effective ice model parameter, N_{bfr} , prefers a value of ~ 0.74 , indicating that the data fits better to an ice model that includes real birefringence effects. For completeness, the explicit results are listed in Table ?. There, the nominal values and the absolute differences to the best fit value are also presented.

Cite (again)! (RED)

Show best fit hole ice angular acceptance compared to nominal and flasher/in-situ fits, maybe? (YELLOW)

2.4.2 Agreement with Standard Model Three-Flavor Oscillation Measurement

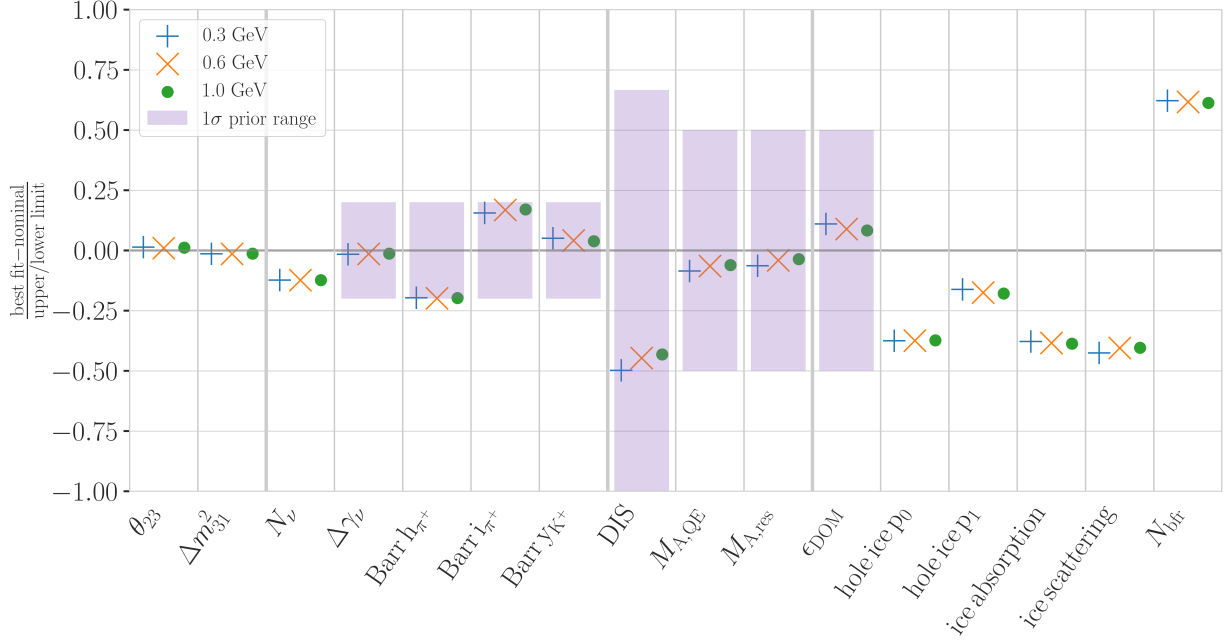


Figure 2.8: Best fit nuisance parameter distances to the nominal values, normalized by the distance to the closest boundary. For parameters with a Gaussian prior, the $+1\sigma$ range is also shown.

The recently performed atmospheric neutrino oscillation measurement by the IceCube collaboration resulted in a best fit point of $\sin^2 \theta_{23} = 0.544^{+0.030}_{-0.096}$ and $\Delta m_{32}^2 = 2.40^{+0.03}_{-0.06} \times 10^{-3} \text{eV}^2$ [10]. The result used the identical 10 years of data at the same final level selection, assuming normal mass ordering. The differences to this analysis are the choice of fit metric and the use of the previous treatment of detector systematic uncertainties. Both the choice of the fit metric and the detector systematic uncertainty treatment should not influence the best fit values and a naive comparison of the results to the results from this work is done, to validate this is the case. The best fit values are listed in Table 2.6 and are all compatible with the IceCube result within the uncertainties. Since they are statistically fully dependent, a more rigorous quantitative comparison would be more involved and is not performed here. The agreement is still interpreted as a first validation of the new detector systematics treatment.

m_4	$\sin^2 \theta_{23}$	$\Delta m_{32}^2 [\text{eV}^2]$
0.3 GeV	0.554	0.0238
0.6 GeV	0.551	0.0238
1.0 GeV	0.553	0.0238

Table 2.6: Best fit oscillation parameters from the three mass sample fits. The values are compatible with the IceCube result within the uncertainties.

[10]: Yu et al. (2023), “Recent neutrino oscillation result with the IceCube experiment”

2.4.3 Best Fit Parameters and Limits

The fitted mixing values are

$$\begin{aligned} |U_{\tau 4}|^2(0.3 \text{ GeV}) &= 0.003^{+0.084}, \\ |U_{\tau 4}|^2(0.6 \text{ GeV}) &= 0.080^{+0.134}, \text{ and} \\ |U_{\tau 4}|^2(1.0 \text{ GeV}) &= 0.106^{+0.132}, \end{aligned}$$

with their $+1\sigma$ uncertainty. All of them are compatible with the null hypothesis of 0.0 mixing, although the 0.6 GeV and 1.0 GeV fits indicate a mixing value of 0.08 and 0.106, respectively. The best fit mixing values and the corresponding upper limits at 68 % and 90 % confidence level (CL) are listed in Table 2.7, also showing the p -value to reject the null hypothesis. The CLs and p -value are estimated by assuming that *Wilks’ theorem* [37] holds, meaning that the TS follows a χ^2 distribution with one degree of freedom.

[37]: Wilks (1938), “The Large-Sample Distribution of the Likelihood Ratio for Testing Composite Hypotheses”

Table 2.7: Best fit mixing values and the corresponding upper limits at 68% and 90% confidence level, as well as the p -value to reject the null hypothesis, estimated by assuming that Wilks' theorem holds.

HNL mass	$ U_{\tau 4} ^2$	68 % CL	90 % CL	NH p -value
0.3 GeV	0.003	0.09	0.19	0.97
0.6 GeV	0.080	0.21	0.36	0.79
1.0 GeV	0.106	0.24	0.40	0.63

Figure 2.9 shows the observed TS profiles as a function of $|U_{\tau 4}|^2$ for all three fits. The TS profile is the difference in χ^2_{mod} between the free fit and a fit where the mixing is fixed to a specific value. Also shown is the expected TS profile, based on 100 pseudo-data trials, produced at the BFP and then fluctuated using both Poisson and Gaussian fluctuations, to include the data and the MC uncertainty as was explained in Section 2.3.2. The Asimov expectation and the 68 % and 90 % bands are shown and the observed TS profiles lie within the 68 % band for all three, confirming that they are compatible with statistical fluctuations of the observed data. For the 0.3 GeV fit, the observed contour is slightly tighter than the Asimov expectation, meaning that the observed upper limits in $|U_{\tau 4}|^2$ are slightly stronger than expected. For the 0.6 GeV the opposite is the case and the observed upper limit is therefore slightly weaker than expected. For the 1.0 GeV fit, the observed upper limit is very close to the Asimov expectation in the region where the 68 % and 90 % CLs thresholds are crossed. The observed upper limits are also shown in Table 2.7.

make summary plot (masses and mixing limits on one) and then discuss wrt to other experiments? (RED)

2.4.4 Comparison to Other Experiments

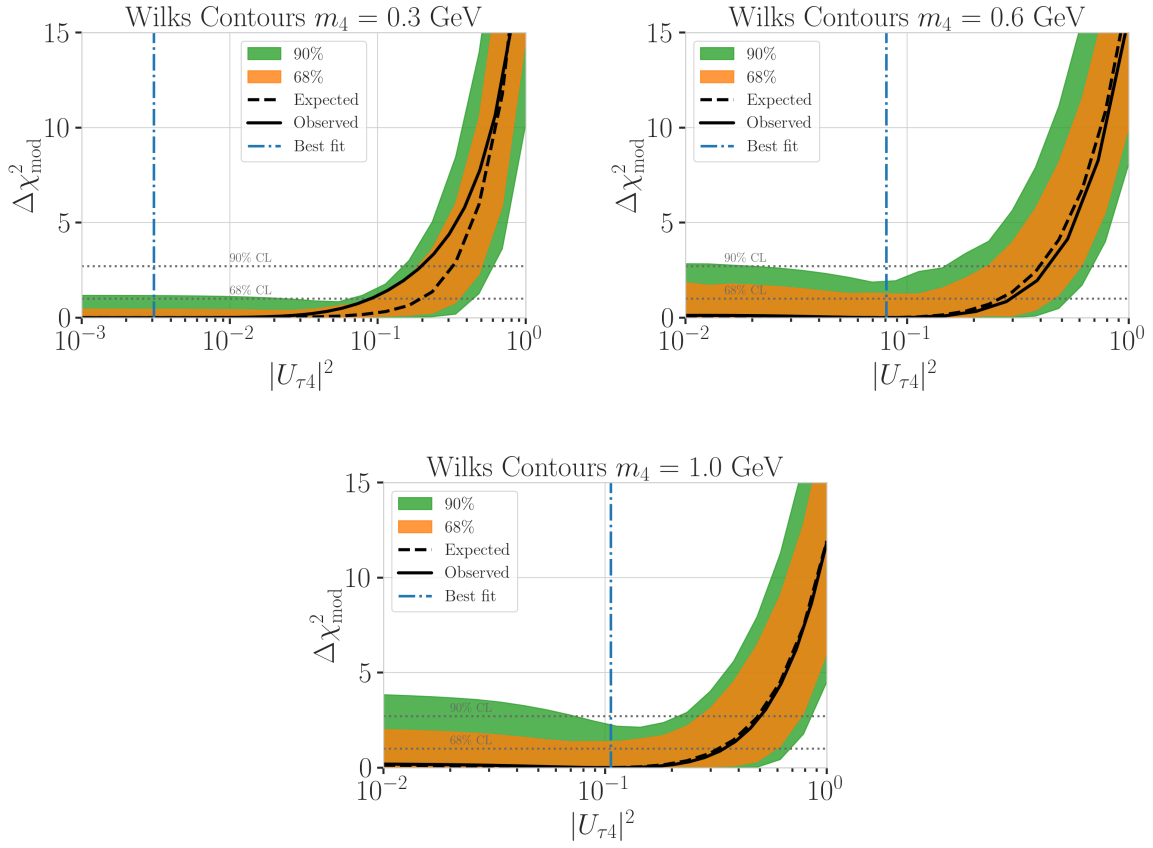


Figure 2.9: Best fit point TS profiles as a function of $|U_{\tau 4}|^2$ for the 0.3 GeV, 0.6 GeV, and 1.0 GeV mass samples. Shown are the observed profiles, the Asimov expectation at the best fit point, and the 68 % and 90 % bands, based on 100 pseudo-data trials. Also indicated are the 68 % and 90 % CL levels assuming Wilks' theorem.

2.5 Outlook

2.5.1 Shape Analysis Improvements

- ▶ estimate full contribution from cascade only events (underestimated due to limited sampling distributions)
- ▶ include double cascade classifier into Binning
- ▶ further optimize binning

2.5.2 Test Coupling to Electron/Muon Flavor

2.5.3 Test Additional Coupling Processes

2.5.4 IceCube Upgrade

List of Figures

1.1	IceCube overview	1
1.2	IceCube side view	2
1.3	Digital optical module (DOM)	3
1.4	IceCube top view	3
1.5	Cherenkov light front	4
2.1	Three dimensional signal over square root of background expectation	11
2.2	Three dimensional background expectation and observed data	12
2.3	Detector systematic uncertainty treatment bin-wise pulls example sets	14
2.4	Nuisance parameter mis-modeling impact ranking	14
2.5	Asimov inject/recover test	17
2.6	Pseudo-data trials fit metric distributions	18
2.7	xx	18
2.8	Best fit nuisance parameter distances to nominal	19
2.9	Best fit point TS profiles	21

List of Tables

1.1	IceCube low energy event signatures and underlying interactions	8
2.1	Final level background event/rate expectation	10
2.2	Final level signal event/rate expectation	10
2.3	Analysis binning	10
2.4	Nuisance parameter nominal values and fit ranges	16
2.5	Staged minimization routine settings	16
2.6	Best fit oscillation parameters	19
2.7	Best fit mixing values and confidence limits	20

Bibliography

Here are the references in citation order.

- [1] M. G. Aartsen et al. “The IceCube Neutrino Observatory: instrumentation and online systems”. In: *Journal of Instrumentation* 12.3 (Mar. 2017), P03012. doi: [10.1088/1748-0221/12/03/P03012](https://doi.org/10.1088/1748-0221/12/03/P03012) (cited on pages 1, 3).
- [2] P. B. Price, K. Woschnagg, and D. Chirkin. “Age vs depth of glacial ice at South Pole”. In: *Geophysical Research Letters* 27.14 (2000), pp. 2129–2132. doi: <https://doi.org/10.1029/2000GL011351> (cited on page 2).
- [3] R. Abbasi et al. “In-situ estimation of ice crystal properties at the South Pole using LED calibration data from the IceCube Neutrino Observatory”. In: *The Cryosphere Discussions* 2022 (2022), pp. 1–48. doi: [10.5194/tc-2022-174](https://doi.org/10.5194/tc-2022-174) (cited on page 2).
- [4] R. Abbasi et al. “The IceCube data acquisition system: Signal capture, digitization, and timestamping”. In: *Nuclear Instruments and Methods in Physics Research Section A: Accelerators, Spectrometers, Detectors and Associated Equipment* 601.3 (2009), pp. 294–316. doi: <https://doi.org/10.1016/j.nima.2009.01.001> (cited on pages 2, 3).
- [5] M. G. Aartsen et al. “Energy Reconstruction Methods in the IceCube Neutrino Telescope”. In: *JINST* 9 (2014), P03009. doi: [10.1088/1748-0221/9/03/P03009](https://doi.org/10.1088/1748-0221/9/03/P03009) (cited on page 3).
- [6] J. Feintzeig. “Searches for Point-like Sources of Astrophysical Neutrinos with the IceCube Neutrino Observatory”. PhD thesis. University of Wisconsin, Madison, Jan. 2014 (cited on pages 3, 15).
- [7] N. Kulacz. “In Situ Measurement of the IceCube DOM Efficiency Factor Using Atmospheric Minimum Ionizing Muons”. MA thesis. University of Alberta, 2019 (cited on pages 3, 15).
- [8] R. Abbasi et al. “The design and performance of IceCube DeepCore”. In: *Astropart. Phys.* 35.10 (2012), pp. 615–624. doi: [10.1016/j.astropartphys.2012.01.004](https://doi.org/10.1016/j.astropartphys.2012.01.004) (cited on page 4).
- [9] R. Abbasi et al. “Measurement of atmospheric neutrino mixing with improved IceCube DeepCore calibration and data processing”. In: *Phys. Rev. D* 108 (1 July 2023), p. 012014. doi: [10.1103/PhysRevD.108.012014](https://doi.org/10.1103/PhysRevD.108.012014) (cited on page 4).
- [10] S. Yu and J. Micallef. “Recent neutrino oscillation result with the IceCube experiment”. In: *38th International Cosmic Ray Conference*. July 2023 (cited on pages 4, 10, 15, 19).
- [11] P. A. Cherenkov. “Visible Radiation Produced by Electrons Moving in a Medium with Velocities Exceeding that of Light”. In: *Phys. Rev.* 52 (4 Aug. 1937), pp. 378–379. doi: [10.1103/PhysRev.52.378](https://doi.org/10.1103/PhysRev.52.378) (cited on page 4).
- [12] V. F. Petrenko and R. W. Whitworth. “214Optical and electronic properties”. In: *Physics of Ice*. Oxford University Press, Jan. 2002. doi: [10.1093/acprof:oso/9780198518945.003.0009](https://doi.org/10.1093/acprof:oso/9780198518945.003.0009) (cited on page 5).
- [13] I. Frank and I. Tamm. “Coherent visible radiation from fast electrons passing through matter”. In: *C. R. Acad. Sci. USSR* 14 (1937), pp. 109–114 (cited on page 5).
- [14] I. Tamm. “Radiation Emitted by Uniformly Moving Electrons”. In: *Selected Papers*. Ed. by B. M. Bolotovskii, V. Y. Frenkel, and R. Peierls. Berlin, Heidelberg: Springer Berlin Heidelberg, 1991, pp. 37–53. doi: [10.1007/978-3-642-74626-0_3](https://doi.org/10.1007/978-3-642-74626-0_3) (cited on page 5).
- [15] L. Rädcl and C. Wiebusch. “Calculation of the Cherenkov light yield from low energetic secondary particles accompanying high-energy muons in ice and water with Geant4 simulations”. In: *Astroparticle Physics* 38 (Oct. 2012), pp. 53–67. doi: [10.1016/j.astropartphys.2012.09.008](https://doi.org/10.1016/j.astropartphys.2012.09.008) (cited on page 5).
- [16] R. L. Workman et al. “Review of Particle Physics”. In: *Progress of Theoretical and Experimental Physics* 2022.8 (Aug. 2022), p. 083C01. doi: [10.1093/ptep/ptac097](https://doi.org/10.1093/ptep/ptac097) (cited on pages 5, 6).

- [17] D. Chirkin and W. Rhode. “Propagating leptons through matter with Muon Monte Carlo (MMC)”. In: (July 2004) (cited on page 5).
- [18] L. Raedel. “Simulation Studies of the Cherenkov Light Yield from Relativistic Particles in High-Energy Neutrino Telescopes with Geant4”. MA thesis. Aachen, Germany: Rheinisch-Westfälischen Technischen Hochschule, 2012 (cited on pages 6, 7).
- [19] M. Tanabashi et al. “Review of Particle Physics”. In: *Phys. Rev. D* 98 (3 Aug. 2018), p. 030001. doi: [10.1103/PhysRevD.98.030001](https://doi.org/10.1103/PhysRevD.98.030001) (cited on page 6).
- [20] E. Longo and I. Sestili. “Monte Carlo Calculation of Photon Initiated Electromagnetic Showers in Lead Glass”. In: *Nucl. Instrum. Meth.* 128 (1975). [Erratum: *Nucl. Instrum. Meth.* 135, 587 (1976)], p. 283. doi: [10.1016/0029-554X\(75\)90679-5](https://doi.org/10.1016/0029-554X(75)90679-5) (cited on page 6).
- [21] S. Agostinelli et al. “Geant4—a simulation toolkit”. In: *Nucl. Instr. Meth. Phys. Res.* 506.3 (July 2003), pp. 250–303. doi: [10.1016/S0168-9002\(03\)01368-8](https://doi.org/10.1016/S0168-9002(03)01368-8) (cited on page 6).
- [22] T. Gabriel et al. “Energy dependence of hadronic activity”. In: *Nuclear Instruments and Methods in Physics Research Section A: Accelerators, Spectrometers, Detectors and Associated Equipment* 338.2 (1994), pp. 336–347. doi: [https://doi.org/10.1016/0168-9002\(94\)91317-X](https://doi.org/10.1016/0168-9002(94)91317-X) (cited on page 7).
- [23] A. Terliuk. “Measurement of atmospheric neutrino oscillations and search for sterile neutrino mixing with IceCube DeepCore”. PhD thesis. Berlin, Germany: Humboldt-Universität zu Berlin, Mathematisch-Naturwissenschaftliche Fakultät, 2018. doi: [10.18452/19304](https://doi.org/10.18452/19304) (cited on page 8).
- [24] V. Barger et al. “Matter effects on three-neutrino oscillations”. In: *Phys. Rev. D* 22 (11 Dec. 1980), pp. 2718–2726. doi: [10.1103/PhysRevD.22.2718](https://doi.org/10.1103/PhysRevD.22.2718) (cited on page 9).
- [25] A. M. Dziewonski and D. L. Anderson. “Preliminary reference Earth model”. In: *Physics of the Earth and Planetary Interiors* 25.4 (1981), pp. 297–356. doi: [https://doi.org/10.1016/0031-9201\(81\)90046-7](https://doi.org/10.1016/0031-9201(81)90046-7) (cited on page 9).
- [26] L. Fischer, R. Naab, and A. Trettin. “Treating detector systematics via a likelihood free inference method”. In: *Journal of Instrumentation* 18.10 (2023), P10019. doi: [10.1088/1748-0221/18/10/P10019](https://doi.org/10.1088/1748-0221/18/10/P10019) (cited on page 13).
- [27] A. Trettin. “Search for eV-scale sterile neutrinos with IceCube DeepCore”. PhD thesis. Berlin, Germany: Humboldt-Universität zu Berlin, Mathematisch-Naturwissenschaftliche Fakultät, 2023. doi: <https://github.com/atrettin/PhD-Thesis> (cited on page 13).
- [28] E. Lohfink. “Testing nonstandard neutrino interaction parameters with IceCube-DeepCore”. PhD thesis. Mainz, Germany: Johannes Gutenberg-Universität Mainz, Fachbereich für Physik, Mathematik und Informatik, 2023. doi: [http://doi.org/10.25358/openscience-9288](https://doi.org/10.25358/openscience-9288) (cited on page 13).
- [29] M. Honda et al. “Atmospheric neutrino flux calculation using the NRLMSISE-00 atmospheric model”. In: *Phys. Rev. D* 92 (2 July 2015), p. 023004. doi: [10.1103/PhysRevD.92.023004](https://doi.org/10.1103/PhysRevD.92.023004) (cited on page 15).
- [30] J. Evans et al. “Uncertainties in atmospheric muon-neutrino fluxes arising from cosmic-ray primaries”. In: *Phys. Rev. D* 95 (2 Jan. 2017), p. 023012. doi: [10.1103/PhysRevD.95.023012](https://doi.org/10.1103/PhysRevD.95.023012) (cited on page 15).
- [31] G. D. Barr et al. “Uncertainties in Atmospheric Neutrino Fluxes”. In: *Phys. Rev. D* 74 (2006), p. 094009. doi: [10.1103/PhysRevD.74.094009](https://doi.org/10.1103/PhysRevD.74.094009) (cited on page 15).
- [32] M. G. Aartsen et al. “Computational techniques for the analysis of small signals in high-statistics neutrino oscillation experiments”. In: *Nucl. Instrum. Meth. A* 977 (2020), p. 164332. doi: [10.1016/j.nima.2020.164332](https://doi.org/10.1016/j.nima.2020.164332) (cited on page 15).
- [33] <https://github.com/icecube/pisa> (cited on page 15).
- [34] R. S. Nickerson. “Confirmation Bias: A Ubiquitous Phenomenon in Many Guises”. In: *Review of General Psychology* 2 (1998), pp. 175–220 (cited on page 16).
- [35] H. Dembinski et al. *scikit-hep/iminuit: v2.17.0*. Version v2.17.0. Sept. 2022. doi: [10.5281/zenodo.7115916](https://doi.org/10.5281/zenodo.7115916) (cited on page 16).
- [36] F. James and M. Roos. “Minuit: A System for Function Minimization and Analysis of the Parameter Errors and Correlations”. In: *Comput. Phys. Commun.* 10 (1975), pp. 343–367. doi: [10.1016/0010-4655\(75\)90039-9](https://doi.org/10.1016/0010-4655(75)90039-9) (cited on page 16).

- [37] S. S. Wilks. “The Large-Sample Distribution of the Likelihood Ratio for Testing Composite Hypotheses”. In: *The Annals of Mathematical Statistics* 9.1 (1938), pp. 60–62. doi: [10.1214/aoms/1177732360](https://doi.org/10.1214/aoms/1177732360) (cited on page 19).